Advanced Robotics

ISSN: 0169-1864 (Print) 1568-5535 (Online) Journal homepage: http://www.tandfonline.com/loi/tadr20

Friction model of fingertip sliding over wavy surface for friction-variable tactile feedback panel

Yohei Fujii, Shogo Okamoto & Yoji Yamada

To cite this article: Yohei Fujii, Shogo Okamoto & Yoji Yamada (2016): Friction model of fingertip sliding over wavy surface for friction-variable tactile feedback panel, Advanced Robotics, DOI: 10.1080/01691864.2016.1208591

To link to this article: http://dx.doi.org/10.1080/01691864.2016.1208591

ADVANCED ROBOTICS, 2016
http://dx.doi.org/10.1080/01691864.2016.1208591

FULL PAPER

Friction model of fingertip sliding over wavy surface for friction-variable tactile feedback panel

Yohei Fujii, Shogo Okamoto and Yoji Yamada

Department of Mechanical Science and Engineering, Nagoya University, Nagoya, Japan

ABSTRACT

A friction-variable touch panel is capable of presenting virtual bumps and holes on its flat surface through the control of the surface friction when a fingertip slides over it. To improve the presentation, we developed a friction model of a fingertip sliding over a sinusoidal surface with an amplitude of 0.5–2.5 mm and a spatial wavelength of 20–50 mm. When a metal ball rolls over a wavy surface with a low friction and contact area, the ratio of the horizontal force to the normal force is equal to the gradient of the surface (this is referred to as the ball bearing model) and is hardly affected by the normal load and rolling speed. In contrast, the profile of the force ratio of a sliding finger is substantially skewed and affected by the sliding direction and normal force exerted by the finger. To model this skewed force ratio, we formulated the asymmetric pressure distribution in the finger-surface contact area and used the effects of the adhesion friction to model the dependency of the force ratio on the normal force and sliding direction. The developed model of a bare finger with these features was found to sufficiently simulate the experimentally observed force ratios. The model can be easily applied to friction-variable touch panels and enables the achievement of a wide variety of haptic contents with macroscopically concave or convex surfaces.

ARTICLE HISTORY
Received 3 August 2015
Revised 13 April 2016
Accepted 1 June 2016

KEYWORDS
Tactile display; finger friction; bump and hole

1. Introduction

Tactile displays that manipulate the friction on their flat panels have attracted much attention in the digital industry mainly because of their good compatibility with touch panels. Such tactile displays include the electrostatic type, which increases the surface friction by the Coulomb forces produced by electric charges,[1,2] and the squeeze-film type, which decreases the surface friction by ultrasound vibrations.[3,4] These friction-variable displays are effective for presenting friction-dominant textures and physical interactions such as non-soft contact by constraining a sliding finger [5] and virtual toggle switching.[3]

However, there are some aspects of tactile displays that require further investigation. An example is the challenge of virtually expressing smooth bumps and holes as large as or larger than a human fingertip on the flat panel. The combination of spatially macroscopic surface profiles and fine textural information, which friction-variable tactile displays are effective for, enables the broadening of the haptic content [6] and thus improves the commercial value of the tactile feedback function. However, to the best knowledge of the authors, a solution to this issue is yet to be proposed, although a vibrotactile approach has been developed.[7,8]

An idea for delivering virtual concave and convex surfaces using friction-variable haptic displays was presented by De-La-Torre and Hayward [9]. As shown in Figure 1, they demonstrated that the perception of bumps and holes can be attributed to normal and tangential sliding forces rather than to the finger displacements caused by the surface curvatures. This indicates that a friction model of the finger and wavy surface would enable the creation of a virtual surface profile even on a flat touch panel. They used a customized force display to demonstrate the perception mechanism. The utilized friction model was simple because the main focus was on the perception phenomena. For the judgment of curvatures, the importance of friction or a resistive force vector in sliding over a curvature was also suggested by Christou and Wing [10]. Other researchers have noted the significant effect of the pressure distribution in the contact area between a fingertip and a curved surface [11–13] or the center of pressure and the gradient of the contact area [13] in the perception of macroscopic surface profiles. One of the friction, gradient of the contact area, or pressure distribution may be effective for the presentation of virtual bumps. Nonetheless, because friction-variable touch panels can only manipulate the surface friction and not the contact area, we employed a

CONTACT Shogo Okamoto okamoto-shogo@nagoya-u.jp

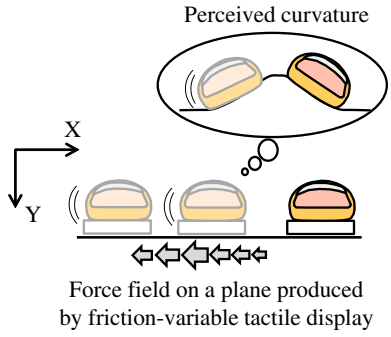

Figure 1. Virtual bump created by a friction field on a flat friction-variable tactile display. Without the *Y*-direction displacement of the finger or surface, the person would vividly feel a bump.

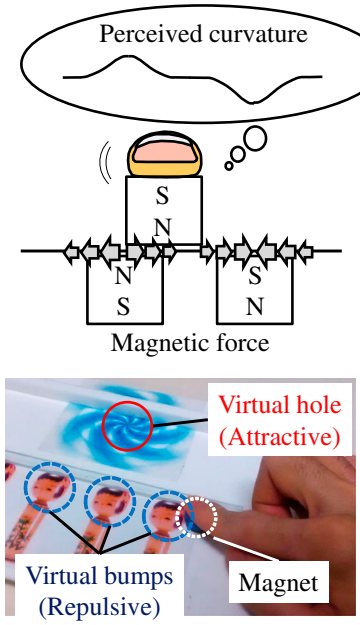

Figure 2. Demonstration of illusory bumps and holes using the force of magnetic fields. The finger slides along a guide bar over a magnet placed on a non-magnetic plate beneath which other magnets are attached. The generated attractive and repulsive force fields, respectively, result in the perception of concave and convex surfaces.

friction-based method. As shown in Figure 2, the virtual bump based on resistive forces can be easily demonstrated by magnets. A plate with magnets attached to its bottom surface is slid by a finger through another magnet. The finger is moved along a linear guide and subjected to repulsive and attractive magnetic forces, resulting in the perception of a bump and hole, respectively, on the plate.

Although magnets produce vivid illusions, the development of a better model for computing the kinetic friction between a finger and a wavy surface would afford higher quality curvature presentation. In addition, the computational load should be made sufficiently small for implementation of the procedure in mobile computers as a background process. Many finger friction models have been studied, some of which are described in the following section. However, most of them were not intended for application to kinetic friction between a finger and wavy profiles. Although some of them may be applied to wavy profiles, attempts were not made to compare the simulation results with the actual frictional forces. The accuracies of the models thus remain uncertain.

In the present study, a model of the kinetic friction between an elastic fingertip and a wavy profile over which the finger slides was developed. By means of the model, friction-variable tactile displays can present virtual macroscopic bumps and holes. To approximate the actual finger friction, the friction produced by an asymmetrically distributed pressure in the finger contact area was expressed in terms of two representative contact points with load-dependent coefficients of friction. In our experiments, the wavy surface was lubricated by talc to reduce the difference between the static and kinetic friction to prevent stick-slip phenomena, which typically induce uncomfortable touch sensations and should be avoided in touch panels with tactile feedback functions. The developed model properly represents the sliding friction of a fingertip and is characterized by a low computational cost, which makes it suitable for mobile terminals with friction-variable tactile displays. The present study was partly based on [14], its unique contributions being the extension of the adopted concept to variable finger loads and comparison of the simulation and actual frictional forces.

2. Related studies on finger friction

In the simulation of grasping using a robotic hand, surface contact between the fingers and the object is not always considered. However, without consideration of the contact area, the frictional constraint would be ineffective, resulting in unstable grasping in the virtual environment. To solve this problem, earlier researchers formulated the conditions for stabilizing the grasp [15] and introduced frictional cones.[16,17] In addition, friction moments [18,19] were used to constrain rotation about the normal to the contact area. However, the modeling of the friction around the contact center in the studies cited in the preceding sentences was different from the frictional behavior observed in the present study.

In some other previous studies, the friction of the surface contact was modeled by multiple contact points. In these other studies, the resultant interaction between the hand and the object was defined by the sum of the forces exerted on the individual contact points.[20,21] For example, Talvas et al. formulated an ellipsoidal contact between a non-flat surface and a virtual finger using

multiple points that adjusted to the curved surface.[21] Although these studies did not discuss the kinetic friction at the contact points, the idea of modeling a contact surface using multiple contact points can also be used to simulate the friction between a fingertip and a curved surface over which the finger slides. However, the results obtained by these methods have not been compared with the actual kinetic friction of a sliding finger. The methods have thus not been used for direct solution of the problem considered in the present study.

Many researchers have also formulated the friction produced by the elastic deformation of a finger,[22–24] although the formulations are not valid for a soft finger that touches an edged surface.[25] Moreover, an attempt has been made to estimate the friction of the fingertip based on the deformation of a circular contact area.[26] These previous works discussed the constraint caused by the finger deformation rather than the sliding friction.

In reality, the actual friction of a sliding fingertip is more complex than those used in the simulation and modeling of robotic grasping. A fingertip is a finite elastic body with epidermal ridges and sweat glands, and some researchers have modeled its true frictional properties. However, the complicated friction phenomena constrained most of these studies to focus on the friction between the fingertip and a flat body.[27] For example, the coefficient of friction under the adhesion and deformation of a fingertip is not constant but a function of the finger load, the sliding velocity and direction, and the sweat condition.[28–33] The dependency of the coefficient of friction of a robotic fingertip on the load has also been investigated.[24,34] The sliding friction produced by a textured surface is vibratory and is composed of up to hundreds of Hertz.[35–37] Moreover, the stick-slip phenomenon of a fingertip is largely random.[38,39] These complicated behaviors of the fingertip are still being actively studied. Finite element models have likewise been used to analyze finger friction,[40,41] although the computational cost may be too high for the utilization of such models in the background processes of mobile terminals.

As noted above, the friction models developed in previous studies cannot be directly applied to the computation of the friction of a fingertip sliding over a convex or concave surface, as in friction-variable tactile displays used in mobile terminals. Although some of the models are potentially applicable to this problem, the goodness of their simulation of actual finger friction is yet to be established. To the best knowledge of the authors, the present study is the first to model the sliding friction of a fingertip on a macroscopically wavy surface.

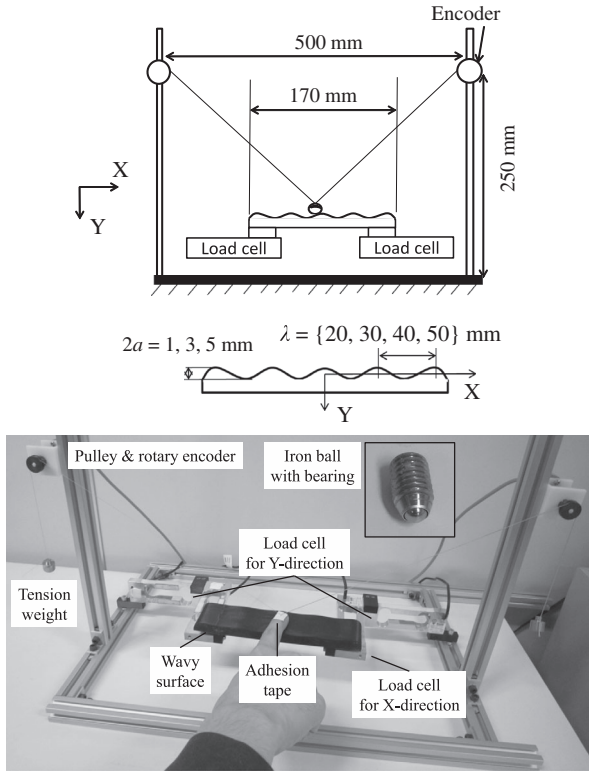

Figure 3. Experimental setup. Top: Schematic of the equipment. Middle: Sinusoidal profile. Bottom: Photograph of the experimental scene.

3. Experiments to observe sliding friction of fingertip on wavy surfaces

3.1. Equipment

We measured the force and position of the finger at 1 kHz using the equipment shown in Figure 3. The main components of the equipment are the four strain-gauge-type load cells (Model 1004, Tedea Huntleigh, USA), which were used to measure the bi-axial forces applied on the wavy surface. The cells were installed such that two were used to measure each axis of the forces. The sinusoidal wavy surface was made from ABS plastic and was finely polished. Its profile was given by the following:

$$y(x) = a\cos\left(\frac{2\pi x}{\lambda}\right) \tag{1}$$

where a and λ are the amplitude and spatial wavelength, respectively. The parameters of the specimens used in the experiment were $a = \{0.5, 1.5, 2.5\}$ and $\lambda = \{20, 30, 40, 50\}$ mm. Two specimens were prepared for each parameter and alternately used. We targeted the surface curvatures that were as large as or larger than that of the human fingertip because it is difficult for friction-variable tactile displays to present finer waves with more than one curvature within the finger contact area.

Two encoders (RE30E-500, Nidec Copal Electronics Corp., Japan) were placed on the sides of the wavy surface to measure the positions of the finger or the ball. The encoders were wound through pulleys by a string taped to the finger or the ball bearing, with resultant position resolutions of 14.4 and 17.2 μm in the X- and Y-direction, respectively.

3.2. Participants and tasks

Three male volunteers with ages ranging between 22 and 30 years participated in the experiment. The widths of their index fingertips were 15, 14, and 14 mm, respectively. As previously noted, talc was used to prevent the finger from sticking to the test surface, thus enabling measurement and modeling of the kinetic friction of the finger. The participants scanned the surface with their index fingers and an iron ball of diameter 6 mm. They repeatedly slid the finger or ball from side to side on the wavy surface for 30 s with arbitrary variation of the scanning velocity and load. They were instructed to maintain the finger posture as much as possible during the sliding.

3.3. Analysis

For all the experimental trials, sample measurements with $f_y \geq 0.6$ N were regarded as valid. Although the test surface was 170 mm long, the central $\pm$30 mm samples were used for the analysis. Although the participants were allowed to scan the surface with any velocity and load, the analysis considered two ranges of the scanning velocity and three ranges of the load to determine the effects of the two parameters. The considered velocities were 5–40 and 40–100 mm/s, and the loads were split into 0.6–1.2, 1.2–1.8, and 1.8–3.0 N. As described below, the scanning velocities were found to hardly affect the results under the present experimental conditions. The samples for all the participants were analyzed together because no significant individual variations were observed. An example of such minor individualities is shown in Section 6.4.

Because the ratios between the X and Y components of the forces are important,[9] we also examined the interactive force with respect to the ratio. The ratio model is practically beneficial for the presentation of virtual bumps and holes in friction-variable tactile displays because it can be used to control the tangential (X-direction) surface friction with respect to the normal (Y-direction) finger force. In the graph shown in Figure 4, the horizontal and vertical axes, respectively, represent the finger or ball position along the X-axis and the force ratio f_x/f_y. The plotted samples were averaged because of the natural variations.

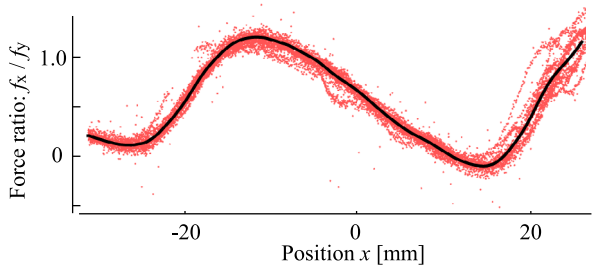

Figure 4. Friction ratio when a participant scanned the wavy surface using his bare finger. The solid line represents the sample average.

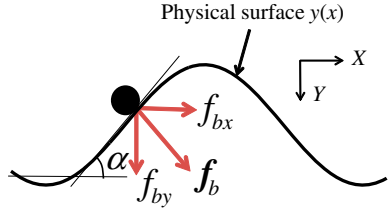

Figure 5. Ball bearing model. The force applied by the ball on the wavy surface is equal to the reaction force of the surface. The ratio between the X- and Y-direction forces is equal to the gradient of the surface.

4. Force ratio of ball rolling on wavy surface

Here, we discuss the force ratios of a ball rolling on the sinusoidal surface. The contact area between the ball and the surface is small and can be considered as a point contact. The rolling friction is also very small. Under these conditions, the ratio between the X- and Y-direction forces is mainly determined by the gradient of the surface, and is described by the simple model used in [9]. This model is referred to as the ball bearing model.

4.1. Ball bearing model

Figure 5 shows the contact between a ball and a sinusoidal surface. The force exerted by the ball ($\boldsymbol{f}_b$) is equivalent to the reaction force of the surface. Under this condition, the ratio of the X-direction force f_{bx} to the Y-direction force f_{by} is equal to the surface gradient, and the following holds:

$$\frac{f_{bx}(x)}{f_{by}(x)} = \frac{dy}{dx} = \frac{|\boldsymbol{f}_b| \sin(\alpha(x))}{|\boldsymbol{f}_b| \cos(\alpha(x))} = \tan(\alpha(x)). \quad (2)$$

Here, $\alpha(x)$ is the gradient of the surface at the contact point x.

4.2. Friction ratio for ball bearing

Figure 6 shows the force ratio when the ball bearing rolls on the surface with $f_y = 1.2$–1.8 N. The left and

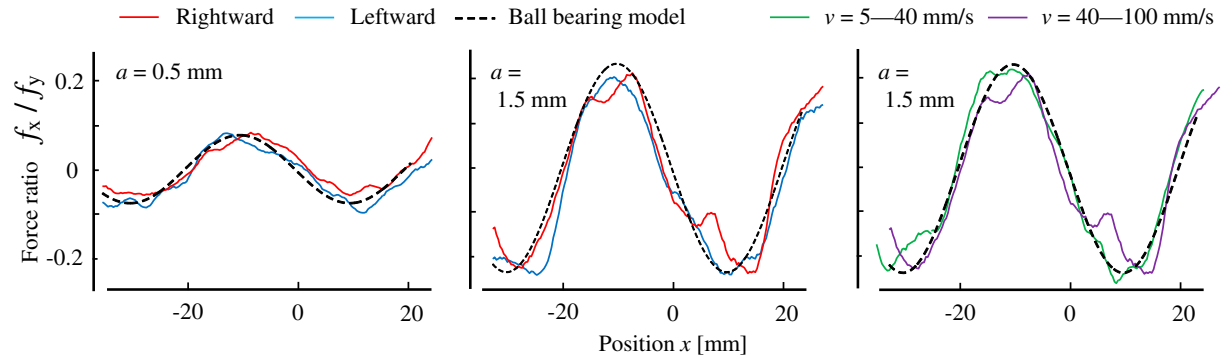

Figure 6. Model-predicted (dotted) and experimentally determined (solid) force ratios of a ball bearing rolling over a sinusoidal surface. Left: For amplitude $a = 0.5$ mm. Middle: For amplitude $a = 1.5$ mm. Right: For 1.5-mm surface and two velocity ranges. The blue and red curves correspond to rightward and leftward rolling of the ball, respectively.

middle figures correspond to surface amplitude a values of 0.5 and 1.5 mm, respectively. The dotted and solid curves represent the gradient of the surface (dy/dx) and the observed force ratio, respectively. The red and blue solid curves represent the force ratios when the surface was scanned in the positive and negative X-directions, respectively. The right figure shows the force ratio for each of the two considered velocity ranges when $a = 1.5$ mm. From the figures and other data not shown in the figures, it was observed that the force ratio matched the prediction of the dotted ball bearing model irrespective of the amplitude of the sinusoidal profile and the rolling direction and velocity. When the contact is nearly a point contact and the friction is small, the ball bearing model fairly represents the actual surface exploration.

5. Force ratio of bare finger sliding over wavy surface

Here, we discuss the force ratio of a fingertip sliding over the surface and show some sample results. Figure 7 shows the force ratios for the sinusoidal profile with $a = 1.5$ mm. Firstly, it should be noted that the profile of the force ratio is not actually sinusoidal but skewed. Secondly, the force ratio is dependent on the sliding direction. The force ratio for the positive X-direction sliding is larger than that determined by the ball bearing model, while that for the negative X-direction sliding is smaller. Furthermore, the force ratio is affected by the normal load of the finger, decreasing with increasing f_y. Below, we discuss the reasons for these observations and establish a friction model for a bare finger sliding over a sinusoidal surface.

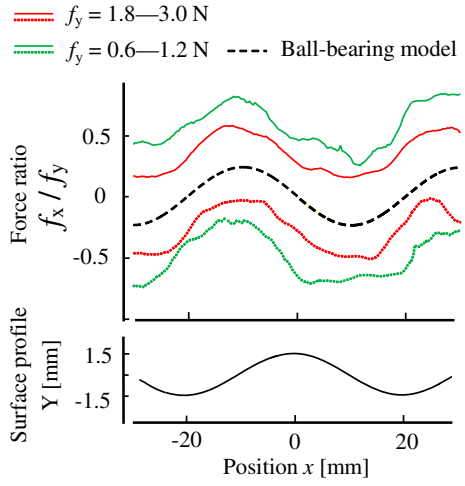

Figure 7. Measured and model-predicted friction ratios of a bare finger sliding over a wavy surface with $a = 1.5$ and $\lambda = 40$ mm. The profiles are not sinusoidal. The absolute measured ratios are mostly larger than those predicted by the ball bearing model and are dependent on f_y. The solid curves correspond to rightward sliding over the surface, while the dotted colored curves correspond to leftward sliding. The bottom panel shows the profile of the wavy surface.

5.1. Skewed force ratio: effect of surface contact

The observed force ratio of the sliding finger is skewed compared to a sinusoidal curve with the rising phase rapid and shorter than the descending phase. The force ratio sharply increases when the finger moves up a slope, and slowly decreases as the top of the curvature is approached and the finger moves down the slope. It is speculated that the deviation of the profile for the finger from that predicted by the ball bearing model is due to the differing contact areas, which are characterized by surface and point contact, respectively. As shown in Figure 8,

on an angled slope, the force distribution in the contact area is asymmetric about the contact center, and this is the cause of the skewed force ratio. A reasonably simple model that expresses this asymmetry is the two-point model that approximates the surface contact between a fingertip and the gradient surface by two representative balls. The model does not express the change in the contact area, but the change in the associated pressure distribution. Nonetheless, because friction-variable tactile displays do not manipulate the contact area or the pressure distribution within it, the purpose of the model is the computation of the resultant frictional forces, to enable the tactile display to render virtual curvatures.

The total force $\boldsymbol{f}_{\mathrm{f}}$ that the finger exerts on the surface at position x is composed of the $\boldsymbol{f}_{\mathrm{b}}$ forces of the two balls. Hence,

$$\boldsymbol{f}_{\mathrm{f}}(x) = \boldsymbol{f}_{\mathrm{b}}(x+r) + \boldsymbol{f}_{\mathrm{b}}(x-r). \tag{3}$$

The distance between the contact center and the ball is denoted by r. On an angled slope, the force distribution in the contact area is asymmetric about the contact center and this is the cause of the skewed force ratio. The normal loads applied by the two balls are not equal; the ball at the higher position on the wavy surface applies a larger normal load:

$$f_{\mathrm{by}}(x+r) > f_{\mathrm{by}}(x-r) \quad \text{if } y(x+r) > y(x-r). \tag{4}$$

The force distribution in the contact area of a finger-like elastic object is largely bell-shaped.[41] Hence, we used the idea of Hertzian contact to represent the force distribution, although a sliding human finger does not exactly exhibit Hertzian contact. As shown in Figure 9, the pressure distribution in the contact area between a spherical and flat body is given by

$$p(r) = p_{\max}\sqrt{1-\left(\frac{r^2}{s}\right)} \tag{5}$$

where $p_{\max}$ and s are the maximum pressure at the center of contact and the radius of the contact area, respectively. When a sphere contacts a flat surface, two points away from the contact center x by $\pm r$ experience equal pressures; that is, $p(x+r) = p(x-r)$. When the surface is inclined at α, the point of maximum pressure shifts by $R\sin(\alpha)$ as shown in the right panel in Figure 9. R is the radius of the sphere. Based on the ratio between the pressures at the two points, the ratio between the Y-direction forces at the two points is

$$f_{\mathrm{by}}(x-r) : f_{\mathrm{by}}(x+r) = \sqrt{1-\left(\frac{-r-R\sin(\alpha(x))}{s}\right)^2} : \sqrt{1-\left(\frac{r-R\sin(\alpha(x))}{s}\right)^2}. \tag{6}$$

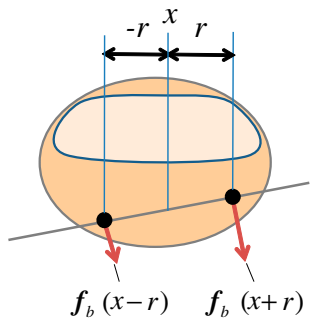

Figure 8. Two balls used to represent the surface contact of a bare finger. The higher ball exerts a larger load.

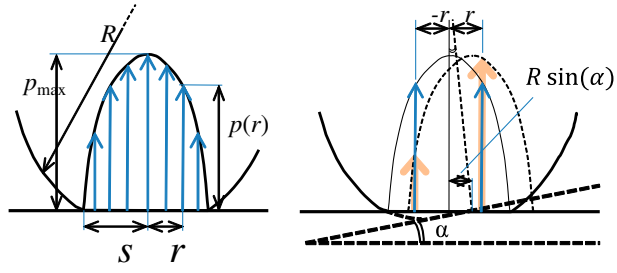

Figure 9. Left: Parabolic pressure distribution on a flat surface. Right: Shift of the center of pressure on an inclined surface.

Hence, the total X-direction force acting on the finger is

$$\begin{aligned} f_{\mathrm{fx}}(x) &= f_{\mathrm{bx}}(x+r) + f_{\mathrm{bx}}(x-r) \\ &= f_{\mathrm{by}}(x+r)\tan(\alpha(x+r)) \\ &\quad + f_{\mathrm{by}}(x-r)\tan(\alpha(x-r)). \end{aligned} \tag{7}$$

In terms of the Y-direction forces, $f_{\mathrm{fy}}(x) = f_{\mathrm{by}}(x-r) + f_{\mathrm{by}}(x+r)$. Hence,

$$f_{\mathrm{by}}(x\pm r) = f_{\mathrm{fy}}(x) \times \frac{\sqrt{1-\left(\frac{\pm r - R\sin(\alpha(x))}{s}\right)^2}}{\sqrt{1-\left(\frac{-r-R\sin(\alpha(x))}{s}\right)^2} + \sqrt{1-\left(\frac{r-R\sin(\alpha(x))}{s}\right)^2}}. \tag{8}$$

The ratio between the X- and Y-direction forces is thus given by

$$\begin{aligned} \frac{f_{\mathrm{x}}(x)}{f_{\mathrm{y}}(x)} &= \frac{f_{\mathrm{by}}(x+r)}{f_{\mathrm{fy}}(x)}\tan(\alpha(x+r)) \\ &\quad + \frac{f_{\mathrm{by}}(x-r)}{f_{\mathrm{fy}}(x)}\tan(\alpha(x-r)). \end{aligned} \tag{9}$$

Figure 10 shows the force ratios for the combined forces of the two balls. With the assumption that the width of the index fingers of the participants is approximately 14 mm, the radius R of the fingertip was set to

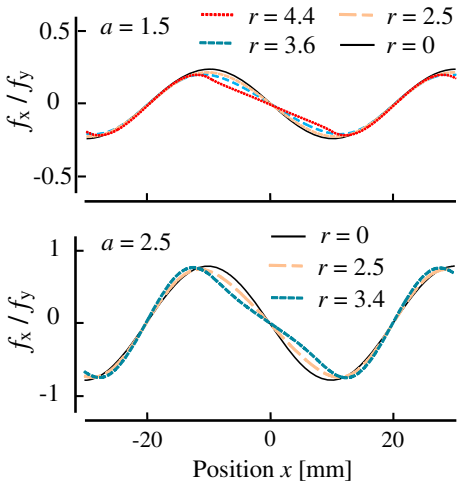

Figure 10. Skewed force ratio. The representation of the fingertip contact by two balls skews the force ratio. $2r$ is the distance between the two balls. The $r = 0$ curve corresponds to the ball bearing model. $R = 7$ mm and $s = 6$ mm.

7 mm. Considering the minor axis radius of the elliptical contact area between the fingertip and the flat surface, s was set to 6 mm. Because of the increasing value of r, which is the distance between the representative ball and the center of contact, the profile of the force ratio becomes more skewed and similar to that for the bare finger.

5.2. Effect of sliding friction

Here, we introduce sliding friction, which is neglected in the ball bearing model. The sliding friction, which is shown in Figure 7, increases the force ratio compared to that obtained by the ball bearing model when the ball slides rightward, whereas it decreases the ratio when the ball slides leftward. Figure 11 shows the forces exerted on the surface with and without considering sliding friction. In the latter case, shown in the left figure, the force ratio is determined by the gradient of the tangent to the curve. In the other case, the interaction force is composed of $\boldsymbol{f}_\mathrm{b}$, which is the equivalent force exerted by the ball bearing, and the sliding friction $\boldsymbol{f}_\mathrm{r}$. If the coefficient of friction is denoted by μ, the sliding friction can be expressed as

$$\boldsymbol{f}_\mathrm{r} = \mu |\boldsymbol{f}_\mathrm{b}| [\cos\alpha, \sin\alpha]^T \tag{10}$$

Therefore, from (2) and (10), the force ratio is obtained as

$$\frac{f_\mathrm{x}(x)}{f_\mathrm{y}(x)} = \frac{|\boldsymbol{f}_\mathrm{b}|\sin\alpha + \mu|\boldsymbol{f}_\mathrm{b}|\cos\alpha}{|\boldsymbol{f}_\mathrm{b}|\cos\alpha - \mu|\boldsymbol{f}_\mathrm{b}|\sin\alpha} = \frac{\tan\alpha + \mu}{1 - \mu\tan\alpha}. \tag{11}$$

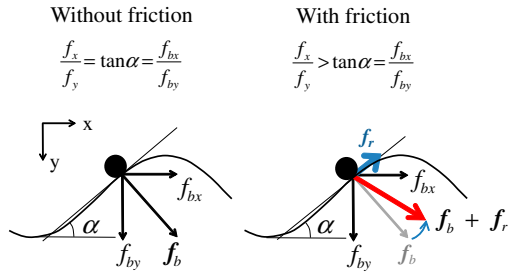

Figure 11. Left: Statically stable ball bearing model without considering friction. Right: Ball bearing model considering friction. $\boldsymbol{f}_\mathrm{r}$ is the sliding friction between the ball and the surface when the ball slides rightward. The resultant force exerted on the surface is the sum of $\boldsymbol{f}_\mathrm{b}$ and $\boldsymbol{f}_\mathrm{r}$.

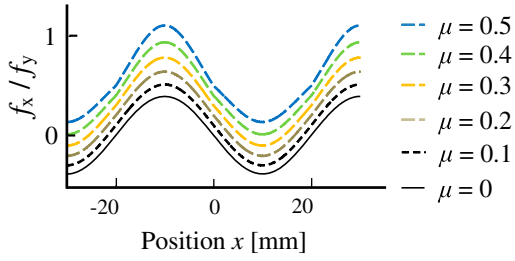

Figure 12. Force ratio of a ball bearing sliding on a wavy surface with varying friction coefficients. When $\mu = 0$, the ratio is equal to that obtained by the ball bearing model.

This force ratio depends on the gradient of the wavy surface and the friction, while the ratio obtained by the ball bearing model is determined by the gradient only, as in (2). It should be noted that the ratio does not depend on the magnitude of the force exerted by the ball, namely, $|\boldsymbol{f}_b|$.

Figure 12 shows the force ratios when the sliding friction is applied to the ball bearing model. With increasing coefficient of friction when the ball slides in the positive X direction, the force ratio is strained and shifts upward. The ratio shifts downward when the ball slides in the negative direction.

5.3. Dependency of friction coefficient on normal force

As previously described, Figure 7 shows that the force ratio depends on the Y direction force. An increase in this force when the finger slides rightward decreases the force ratio. This is because of the dependency of the coefficient of friction on the force. In the case of a finger that slides over a smooth rigid body, as in the present experiment, the friction is mainly composed of the deformation and adhesion friction. The behaviors of the coefficients of friction for these two types of frictions differ. The coefficient of friction for the adhesion friction is a negative power function of the force applied by the finger, whereas that

for the deformation friction is a positive power function of the finger force.[28,29] Regarding the contributions of these two types of frictions for a sliding finger, the adhesion friction is dominant under dry conditions,[30,42] whereas the deformation friction plays a slightly more dominant role under lubricated conditions.[30] Hence, the general form of the coefficient of friction can be written as

$$\mu \propto |\boldsymbol{f}_{\mathrm{b}}|^{n} \tag{12}$$

where n can be either positive, negative, or zero depending on the tribological system.

5.4. Bare finger model

By incorporating the above characteristics, the force ratio when a bare finger slides over a sinusoidal surface can be described as follows based on (9), (11), and (12):

$$\frac{f_{\mathrm{x}}(x)}{f_{\mathrm{y}}(x)} = \frac{f_{by}(x+r)}{f_{fy}(x)} \frac{\tan\left(\alpha(x+r)\right) + \mu|\boldsymbol{f}_{\mathrm{b}}|^{n}}{1 - \mu|\boldsymbol{f}_{\mathrm{b}}|^{n}\tan\left(\alpha(x+r)\right)} + \frac{f_{by}(x-r)}{f_{fy}(x)} \frac{\tan\left(\alpha(x-r)\right) + \mu|\boldsymbol{f}_{\mathrm{b}}|^{n}}{1 - \mu|\boldsymbol{f}_{\mathrm{b}}|^{n}\tan\left(\alpha(x-r)\right)}. \tag{13}$$

6. Comparison of simulation and observed friction ratios

Here, we compare the experimentally observed force ratio with that determined by simulation using the bare finger model.

6.1. Parameters of simulation force ratio

The parameters of the model were set as follows: $R = 7\,\mathrm{mm}$, $r = 3.4\,\mathrm{mm}$, $s = 6\,\mathrm{mm}$, $\mu = 0.4$, and $n = -0.3$. With the exception of the R and s values, the parameters were searched for such that the simulation and actual force ratios would be comparable for $\lambda = 40\,\mathrm{mm}$.

As previously noted, a larger r further skews the force ratio. We evaluated the degree of skewness based on the proportion of the downward curve of the force ratio to the upward curve. The value of r that made the proportion for the simulation very similar to that for the experiment was searched for within 0–6 mm using increments of 0.1 mm.

Furthermore, the coefficient of friction μ, which mainly determines the degree of the base shift of the force ratio, and the power value n, which indicates the dependency of the coefficient of friction on the finger load, were varied within 0–0.5 and −0.5–0.5, respectively, to make the center levels of the simulation and actual force ratios as close as possible. The final values were $\mu = 0.4$, which is within the range of the coefficients of friction between the human skin and common materials,[27] and $n = -0.3$.

6.2. Comparison of general features with varying wave heights and finger loads

Figure 13 shows the force ratio for each amplitude of the sinusoidal profile for $\lambda = 40\,\mathrm{mm}$.

As previously mentioned, the profiles of the force ratios for a bare finger and a ball bearing differ significantly. The force ratio for a finger rises rapidly and falls slowly, whereas that for a ball bearing has equally long rising and falling phases. Although our bare finger model fairly exhibits the skewed trend, its force ratio does not completely match the actual value, especially for $a = 2.5$ mm, in which case the actual force ratio is larger than that of the model.

Friction shifts the base line of the force ratio. When the finger slides in the positive X direction, the force ratio shifts upward and vice versa. This trend was clearly observed in the experiment, and was well represented by the bare finger model.

In addition, the actual force ratio depends on the finger load, with a smaller load increasing the force ratio. Under our experimental conditions, the coefficient of friction is a negative power function of the load because the adhesion friction is dominant. The adhesion friction between a sphere and an elastic plate is proportional to the two-third power of the load,[28] while the coefficient of friction is proportional to the negative one-third power of the load. The exponent n used above was −0.3, which is close to $-1/3$. Consequently, the bare finger model produced a negative correlation between the normal load and the magnitude of the force ratio.

In the experiment, the force ratio was hardly affected by the sliding velocity. This was not unexpected because the adhesion friction between elastic and rigid bodies rarely depends on the sliding velocity.[30]

6.3. Comparison for various surface wavelengths

In this section, we compare the simulation and experimental results for $\lambda = 20$, 30, and 50 mm. The above-mentioned results were for $\lambda = 40\,\mathrm{mm}$.

As can be observed from Figure 14, the simulation profiles also agree well with the experimental results for $\lambda = 30$ and 50 mm (middle and right). The same simulation parameters used for $\lambda = 40\,\mathrm{mm}$ were adopted for these cases. As can be seen from the plots, when the width of the bumps or holes is larger than that of the fingertip, or the surface gradient is small, our model successfully predicts the actual interaction forces. This is because the model presumes sufficiently small surface gradients such

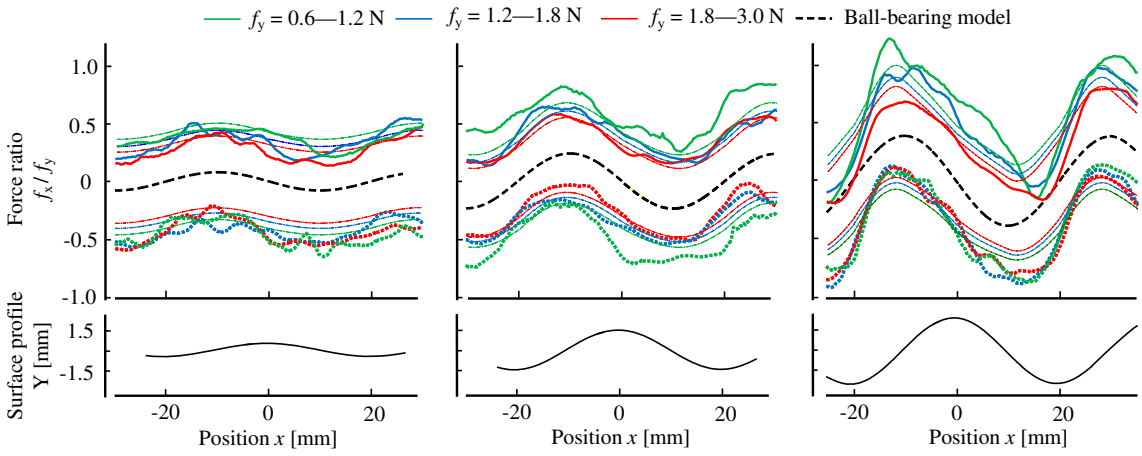

Figure 13. Force ratio of sliding finger. The fine curves represent the simulation results, while the solid and dotted bold curves, respectively, correspond to rightward and leftward sliding of the finger. The black dotted curves represent the force ratio of the ball bearing model. Left: $a = 0.5$ mm. Center: $a = 1.5$ mm. Right: $a = 2.5$ mm. The other simulation parameters were as follows: $R = 7$ mm, $r = 3.4$ mm, $s = 6.0$ mm, $\mu = 0.4$, and $n = -0.3$. The employed value of f_y for the simulation was the median of each range.

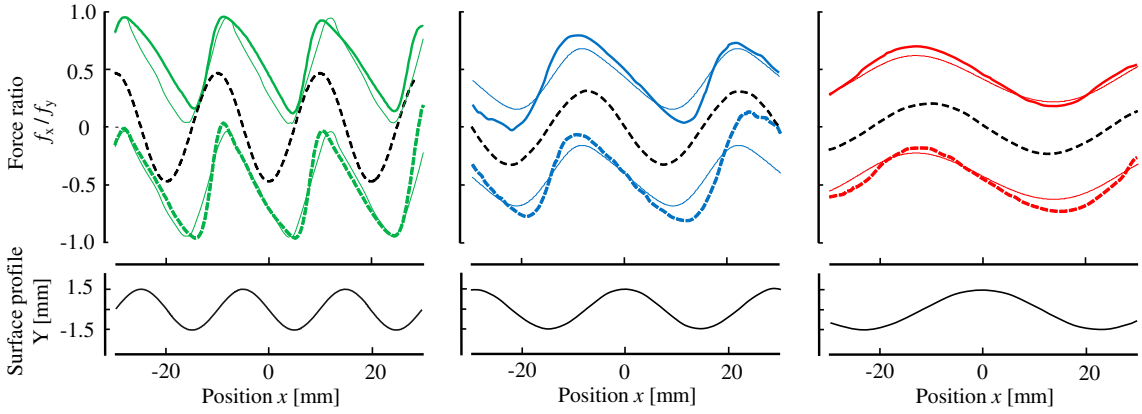

Figure 14. Force ratio of sliding finger. The fine curves represent the simulation results, with the solid and dotted bold curves, respectively, corresponding to rightward and leftward sliding of the finger. The black dotted curves represent the force ratio of the ball bearing model. Left: $\lambda = 20$ mm ($r = 2.2$ mm, $s = 5.0$ mm). Center: $\lambda = 30$ mm ($r = 3.4$ mm, $s = 6.0$ mm). Right: $\lambda = 50$ mm ($r = 3.4$ mm, $s = 6.0$ mm). The height a of the wavy surfaces was 1.5 mm. The other simulation parameters were as follows: $R = 7$ mm, $\mu = 0.4$, and $n = -0.3$. The f_y value for the simulation was 1.0 N, which is the median of the finger loads used for the computation.

that the contact area of the finger does not significantly vary while scanning the bumpy surfaces.

However, for a smaller bump width, as in the case of $\lambda = 20$ mm, different simulation parameters were needed to be selected. Using the procedure described in Section 6.1, the simulation parameters for this case were set to $r = 2.2$ and $s = 5.0$ mm. These values are smaller than those used for the other cases with larger λ values. Because the surface gradient for $\lambda = 20$ mm was steeper than those for the other cases, the parameters related to the contact area were needed to be adjusted accordingly.

6.4. *Individual variance of force ratios*

Finally, in Figure 15, we present the individuality of the force ratio when the participants scanned the sinusoidal profile for $\lambda = 40$ mm and $a = 0.5$ mm with $f_y = 1.2$–1.8 N. One additional participant (Participant D) with a fingertip width of 14 mm was invited for the purpose, i.e. in addition to the three participants of the previous experiments. The differences among the individual force ratiocurves are apparently minor although there are subtle biases that may be attributed to the varying forces applied by the participants. Such relatively minute individual differences might have been due to the control of the experimental conditions. Particularly, talc was effective for maintaining dry conditions.

7. Discussion

We modeled the ratio between the X- and Y-direction forces applied by a fingertip sliding over a sinusoidal

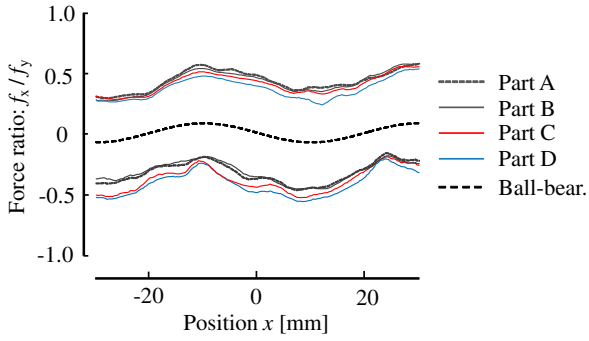

Figure 15. Force ratio curves for the four participants. A sinusoidal surface with $\lambda = 40$ mm and $a = 0.5$ mm was explored with a finger load f_y of 1.2–1.8 N.

surface. Whereas the model can still be improved, it is useful for the presentation of macroscopic surface profiles on friction-variable tactile panels.

7.1. Expression of asymmetric pressure distribution

We considered that the skewed force ratio of a sliding finger indicates that the pressure in the contact area is not symmetric about the center of contact. We used a pressure distribution model based on Hertzian theory to describe this asymmetry although the physical plausibility or correctness of this modeling is uncertain and other approaches may be available. For example, the deformation of the contact surface of an elastic body under a tangential force has been formulated,[43] and such a formula is used to define the asymmetric pressure distribution as a function of the tangential force, whereas it was determined from the gradient of the surface in the present study.

7.2. Limitations of friction model

As stated in Section 6.3, the prediction of the actual interaction forces using our model requires adjustment of the simulation parameters with respect to the surface profile. The detailed relationship between these parameters and the surface profile requires further study. Additionally, our proposed method is not applicable to some surfaces because of the assumptions that the model is based on.

First, the skewness of the actual force ratio for a surface amplitude of 2.5 mm was unexpectedly large, compared to the predictions of our model. This discrepancy can be explained by the fact that, when the amplitude of the wavy surface is as large as 2.5 mm, the fingertip may fit into the hole as shown in Figure 16(a), thereby increasing the contact area, and hence the coefficient of friction. Consequently, the values of s and μ may vary with the macroscopic surface profile, whereas constant values were employed in our simulation.

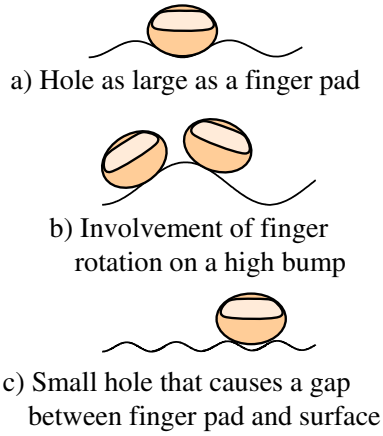

Figure 16. Cases with limited applicability of the proposed model. (a) The fingertip fits into a hole, resulting in irregular increase in the contact area. (b) The fingertip rotates on a large bump, resulting in violation of the model assumption that the fingertip remains horizontal. (c) The interval between neighboring bumps is smaller than the fingertip, resulting in the finger pad simultaneously contacting more than one bump.

Second, in our model, the posture of the finger remains horizontal during the scanning. However, this assumption is unlikely to hold when the surface gradient is large, as shown in Figure 16(b), in which case the finger may rotate on the surface. Hence, it is speculated that the friction model will not accurately present the force ratio for a large bump.

Finally, as previously mentioned, our model targets macroscopic surface roughness or profiles, for which the width of a bump is larger than that of the fingertip. For this purpose, it is assumed that the finger pad contacts the surface with no gap. As the surface wave becomes finer, the finger simultaneously contacts multiple bumps and a non-contacted gap is developed, as shown in Figure 16(c). In this case, our model is inapplicable.

7.3. Presentation of surface bumps and holes through friction-variable touch panel

Our model was aimed at presenting virtual bumps and holes by means of a friction-variable touch panel. For this purpose, the friction force is computed by multiplying the measured normal load by the force ratio determined by the developed model. Although most currently available commercial touch panels do not have force detection functions, such functions are expected to become part of the general specifications when tactile feedback displays become prevalent. One advantage of curvature presentation using our model is that the panel does not need to be able to increase and decreaseits surface friction from its neutral value. In the ball bearing model, the force ratio range includes zero and

the touch panel therefore needs to output both resistive and assistive friction. Unfortunately, such bidirectional friction variation can only be realized by combining more than two different mechanisms. In contrast, the actual force ratio of a fingertip does not necessarily cross zero and can be presented by simply increasing the friction. From this perspective, an electrostatic-type friction-variable display is suitable for the presentation of virtual waves. Indeed, there has been a previous study [44] in which virtual bumps were rendered using the ball bearing model and an electrostatic-type display with limited capabilities. Furthermore, the amplitudes of virtualbumps or holes perceived by friction may be smaller than the values employed in a model because a touch panel does not induce normal displacements on its surface. However, it is obvious that the combined use of a frictional cue by a tactile display and a visual cue would facilitate effective presentation of virtual bumps and holes.

8. Conclusion

Based on the illusory perception of macroscopic concave and convex surfaces by the tangential force of a sliding finger without movement in the normal direction, wedeveloped a friction model for the presentation of virtual bumps and holes on the flat surface of a friction-variable tactile feedback panel. No previous model could be directly used for this purpose. Although a number of studies on finger friction have been conducted,most of them did not address the kinetic friction of a fingertip sliding over a macroscopically wavy surface. In addition, while a few of the developed models may be extended to serve our purpose, the predictions of the models were not compared with the actual sliding friction of the finger. In the present study, we observed the ratios between the X- and Y-direction forces applied by an iron ball and a fingertip sliding over a surface with a sinusoidal profile. The force ratio for the ball, which had a very small contact area and rolling friction matched the gradientof the surface irrespective of the magnitudes of the forces and the rolling velocity. This force ratio was referred to as the ball bearing model. The force ratio of the fingertip did not match the ball bearing model but had a skewed profileand a shifted base level that depended on the sliding direction and finger force. We consequently developed a bare finger model that described the skewed force ratio based on the asymmetric pressure distribution in the contact area. The model further incorporated the adhesion friction to consider the dependency of the ratio on the normal force. By manual adjustment of its parameters, the bare finger model fairly represents the actual force ratio of the human finger.

Disclosure statement

No potential conflict of interest was reported by the authors.

Funding

This study was in part supported by MIC SCOPE [27-J-J6238]; KAKENHI Shitsukan [15H05923].

Notes on contributors

Yohei Fujii received a MS degree in engineering from Nagoya University in 2016. His research interests comprise energy engineering and haptics.

Shogo Okamoto received MS and PhD degrees in information sciences in 2007 and 2010, respectively, from the Graduate School of Information Sciences, Tohoku University. Since 2010, he has been with the Department of Mechanical Science and Engineering, Nagoya University, Japan. His research interests comprise haptics, human assistive technology, and wearable robots.

Yoji Yamada received a PhD degree from the Tokyo Institute of Technology in 1990. He has been an associate professor at the Toyota Technological Institute, Japan since 1983. In 2004, he joined the National Institute of Advanced Industrial and Science Technology (AIST), as a group leader of the Safety Intelligence Research Group at the Intelligent Systems Research Institute. In 2008, he moved to the Graduate School of Engineering, Nagoya University, as a professor.

References

[1] Nakamura T, Yamamoto A. Multi-finger electrostatic passive haptic feedback on a visual display. In: Proceedings of IEEE World Haptics Conference. Daejeon; 2013. p. 37–42.
[2] Bau O, Poupyrev I. REVEL: tactile feedback technology for augmented reality. In: Proceedings of SIGGRAPH. Vol. 31. Los angeles (CA); 2012. p. 89.
[3] Chubb EC, Colgate JE, Peshkin MA. ShiverPaD: a glass haptic surface that produces shear force on a bare finger. IEEE Trans. Haptics. 2010;3:189–198.
[4] Biet M, Boulon L, Martinot F, et al. Evidence for an anisotropic deprivation of frictional cues in microtexture

perception. In: Proceedings of IEEE World Haptics Conference. Tsukuba; 2007. p. 385–390.
[5] Nakamura T, Yamamoto A. Built-in capacitive position sensing for multi-user electrostatic visuo-haptic display. In: Kajimoto H, Ando H, Kyung KU, editors. Devices and applications. Vol. 277, Lecture notes in electrical engineering. Berlin: Springer; 2014. p. 183–185.
[6] Saga S, Raskar R. Simultaneous geometry and texture display based on lateral force for touchscreen. In: Proceedings of the IEEE World Haptics Conference. Daejeon; 2013. p. 437–442.
[7] Tsuchiya S, Konyo M, Yamada H, et al. Virtual active touch II: vibrotactile representation of friction and a new approach to surface shape display. In: Proceedings of IEEE/RSJ International Conference on Intelligent Robots and Systems. St. Louis (MO); 2009. p. 3184–3189.
[8] Tsuchiya S, Konyo M, Yamada H, et al. Vib-touch: virtual active touch interface for handheld devices. In: Proceedings of IEEE International Symposium on Robot and Human Interactive Communication. Toyama; 2009. p. 12–17.
[9] Robles-De-La-Torre G, Hayward V. Force can overcome object geometry in the perception of shape through active touch. Nature. 2001;412:445–448.
[10] Christou C, Wing A. Friction and curvature judgement. In: Proceedings of EuroHaptics. Birmingham; 2001. p. 36–40.
[11] Goodwin AW, John KT, Marceglia AH. Tactile discrimination of curvature by humans using only cutaneous information from the fingerpads. Exp. Brain Res. 1991;86:663–672.
[12] Goodwin AW, Wheat HE. Human tactile discrimination of curvature when contact area with the skin remains constant. Exp. Brain Res. 2013;88:447–450.
[13] Wijntjes MWA, Sato A, Hayward V, et al. Local surface orientation dominates haptic curvature discrimination. IEEE Trans. Haptics. 2009;2:94–102.
[14] Fujii Y, Okamoto S, Yamada Y. Interactive forces caused by scanning wavy surfaces. In: Proceedings of IEEE Haptics Symposium. Houston; 2014. p. 449–453.
[15] Cole ABA, Hauser JE, Sastry SS. Kinematics and control of multifingered hands with rolling contac. IEEE Trans. Autom. Control. 1989;34:398–404.
[16] Harwin WS, Melder N. Improved haptic rendering for multi-finger manipulation using friction cone based god-objects. In: Proceedings of EuroHaptics. Edinburgh;2002. p. 82–85.
[17] Ruspini DC, Kolarov K, Khatib O. The haptic display of complex graphical environments. In: Proceedings of SIGGRAPH. Los Angeles (CA); 1997. p. 345–352.
[18] Barbagli F, Frisoli A, Salisbury K, et al. Simulating human fingers: a soft finger proxy model and algorithm. In: Proceedings of IEEE Haptics Symposium. Chicago; 2004. p. 9–17.
[19] Borst C, Indugula A. Realistic virtual grasping. In: Proceedings of the IEEE Virtual Reality Conference. Bonn; 2005. p. 12–16.
[20] Jacobs J, Froehlich B. A soft hand model for physically-based manipulation of virtual objects. In: Proceedings of IEEE Virtual Reality Conference. Singapore; 2011. p. 11–18.
[21] Talvas A, Marchal M, Lécuyer A. The god-finger method for improving 3D interaction with virtual objects through simulation of contact area. In: Proceedings of IEEE Symposium on 3D User Interfaces. Orlando; 2013. p. 111–114.
[22] Inoue T, Hirai S. Parallel-distributed model of soft fingertips in three-dimensional grasping and manipulation. In: Proceedings of IEEE International Conference on Robotics and Biomimetics. Bangkok; 2008. p. 895–902.
[23] Arimoto S, Tahara K, Yamaguchi M, et al. Principles of superposition for controlling pinch motions by means of robot fingers with soft tips. Robotica. 2001;19:21–28.
[24] Tiezzi P, Kao I, Vassura G. Effect of layer compliance on frictional behavior of soft robotic fingers. Adv. Robot. 2007;21:1653–1670.
[25] Watanabe T, Fujihira Y. Experimental investigation of effect of fingertip stiffness on friction while grasping an object. In: Proceedings of IEEE International Conference on Robotics and Automation. Hong Kong; 2014. p. 889–894.
[26] Kurita Y, Yonezawa S, Ikeda A, et al. Weight and friction display device by controlling the slip condition of a fingertip. In: Proceedings of IEEE/RSJ International Conference on Intelligent Robots and Systems. San Francisco (CA); 2011. p. 2127–2132.
[27] Derler S, Gerhardt LC. Tribology of skin: review and analysis of experimental results for the friction coefficient of human skin. Tribol. Lett. 2012;45:1–27.
[28] Adams MJ, Briscoe BJ, Johnson SA. Friction and lubrication of human skin. Tribol. Lett. 2007;26:239–253.
[29] Derler S, Gerhardt LC, Lenz A, et al. Friction of human skin against smooth and rough glass as a function of the contact pressure. Tribol. Int. 2009;42:1565–1574.
[30] Mahdi D, Riches A, Gester M, et al. Rolling and sliding: separation of adhesion and deformation friction and their relative contribution to total friction. Tribol. Int. 2015;89:128–134.
[31] Adams MJ, Johnson SA, Lefèvre P, et al. Finger pad friction and its role in grip and touch. J. R. Soc. Interface. 2013;10:20120467.
[32] Dzidek BM, Adams M, Zhang Z, et al. Role of occlusion in non-coulombic slip of the finger pad. In: Auvray M, Duriez C, editors. Haptics: Neuroscience, devices, modeling, and applications. Vol. 8618, Lecture notes in computer science. Berlin: Springer; 2014. p. 109–116.
[33] Han HY, Shimada A, Kawamura S. Analysis of friction on human fingers and design of artificial fingers. In: Proceedings of IEEE International Conference on Robotics and Automation. Vol. 4. Minneapolis (MN); 1996. p. 3061–3066.
[34] Cutkosky MR, Jourdain JM, Wright PK. Skin materials for robotic fingers. In: Proceedings of IEEE International Conference on Robotics and Automation. Vol. 4. Raleigh; 1987. p. 1649–1654.
[35] Fagiani R, Massi F, Chatelet E, et al. Tactile perception by friction induced vibrations. Tribol. Int. 2011;44:1100–1110.
[36] Smith AM, Chapman CE, Deslandes M, et al. Role of friction and tangential force variation in the subjective scaling of tactile roughness. Exp. Brain Res. 2002;144:211–223.

[37] Nakano K. Information regarding tactile sensation in friction signals with high uncertainty. Tribol. Int. 2008;41:1114–1125.
[38] Terekhov AV, Hayward V. Minimal adhesion surface area in tangentially loaded digital contacts. J. Biomech. 2011;44:2508–2510.
[39] Derler S, Rotaru GM. Stick-slip phenomena in the friction of human skin. Wear. 2013;302:324–329.
[40] Ho VA, Hirai S. Modeling and analysis of a frictional sliding soft fingertip, and experimental validations. Adv. Robot. 2012;25:291–311.
[41] Maeno T, Kawamura T, Cheng S-C. Friction estimation by pressing an elastic finger-shaped sensor against a surface. IEEE Trans. Robot. Autom. 2004;20:222–228.
[42] Masen MA. A systems based experimental approach to tactile friction. J. Mech. Behav. Biomed. Mater. 2011;4:1620–1626.
[43] Johnson KL. Contact mechanics. Cambridge (UK): Cambridge University Press; 1987.
[44] Kim SC, Israr A, Poupyrev I. Tactile rendering of 3D features on touch surfaces. In: Proceedings of ACM Symposium on User Interface Software and Technology. St. Andrews; 2013. p. 531–538.